Journal of Power Sources 204 (2012) 67–73

Contents lists available at SciVerse ScienceDirect

Journal of Power Sources

journal homepage: www.elsevier.com/locate/jpowsour

Short communication

Optimization of anode material composed of Y-doped $SrTiO_3$ and metal and/or oxide additives for solid oxide fuel cells

Pramote Puengjinda, Hiroki Muroyama, Toshiaki Matsui, Koichi Eguchi*

Department of Energy and Hydrocarbon Chemistry, Graduate School of Engineering, Kyoto University, Nishikyo-ku, Kyoto 615-8510, Japan

ARTICLE INFO

Article history:
Received 31 August 2011
Received in revised form
16 December 2011
Accepted 19 December 2011
Available online 29 December 2011

Keywords:
Solid oxide fuel cells
Ceramic anodes
Catalyst impregnation
Carbon tolerance

ABSTRACT

Y-doped $SrTiO_3$ (YST) is currently used as an effective anode component to solve the shortcomings of conventional Ni-based cermet anodes. In this study, YST-based composite with a different ceramic oxide including samaria-doped ceria (SDC) or yttria-stabilized zirconia (YSZ) was developed as an anode material to evaluate the electrocatalytic performance in hydrogen and methane fuels. The composites showed a good potential in electrical conductivity and compatibility with YSZ electrolyte in the anodic condition. The cell with YST–SDC anode attained the better performance than that with YST–YSZ anode, which was ascribable to the high electrical conductivity and electrocatalytic activity of SDC towards the oxidation of fuels. Addition of nickel remarkably enhanced the electrochemical performance and the stability of the anodes. With 10 wt% of nickel oxide loading, the performance was significantly increased under the operation in humidified hydrogen and methane. Note that in methane fuel, the performance deterioration has not been observed over the short-term operation for 20 h.

1. Introduction

Solid oxide fuel cells (SOFCs) have been currently considered as one of the promising power generation systems due to their clean and efficient generation process as compared to the internal combustion engines. Because of the higher energy conversion efficiency and the potential for co-generation of heat and electricity, many efforts have been devoted to commercialize SOFCs. A porous composite of Ni and ceramic is widely used as a cermet anode, which typically contains a high volume fraction of Ni to form the electronic percolation path and expand the elctrocatalytically active region in the electrode. However, such high Ni fraction in the anode results in a serious mechanical failure due to the volume change of Ni phase upon redox cycles. In addition, the Ni-based cermet anode is also unfavorable for the direct utilization of hydrocarbon fuels because the carbon deposition is catalytically promoted over Ni metal [1–3]. From these reasons, it is necessary to develop alternative anode materials to overcome the problems associated with the conventional Ni-based cermets. Alternative materials such as doped $LaCrO_3$ [4,5], doped $SrTiO_3$ [6], Cu—CeO_2, Ru—CeO_2 [7–9], *etc.* have been developed. Among them, doped $SrTiO_3$ ceramic including lanthanum- or yttria-doped $SrTiO_3$ ($La_xSr_{1-x}TiO_3$ (LST) or $Y_xSr_{1-x}TiO_3$ (YST)) is one of the potential candidates for anode materials because of the high electronic conductivity under reducing conditions [4,5,10–14]. Their ionic conductivity and catalytic activity for the fuel oxidation, however, are relatively lower than those of the Ni-based cermets. Therefore, for the enhancement of electrocatalytic activity of ceramic anodes, it is essential to add a promoter material with high ionic conductivity and catalytic activity such as ceria-based oxide [15,16], zirconia-based oxide, and a small amount of nickel [10], *etc.* Although many researchers have reported advantages of the electron-conductive ceramics and their composites, the evaluation of these materials as anodes on the stability under various operating conditions has not been conducted extensively. Recently, Ikebe et al. evaluated the performance of the composite anode consisting of YST, yttria-stabilized zirconia (YSZ), and Ni, which mainly served as an electronic conductor, an oxide ion conductor, and a catalyst for the hydrogen oxidation, respectively [10]. The cell with this composite anode exhibited stable performance at the constant terminal voltage of 0.7 V in humidified hydrogen (0.6% H_2O—H_2) for 21 h. In addition, the cell performance remained unchanged even after five consecutive redox cycles mainly due to the stable porous framework of YST–YSZ with low Ni content.

In this study, then, we fabricated the composite anode of YST with an ion-conductive oxide such as samaria-doped ceria (SDC) and yttria-stabilized zirconia (YSZ). The effect of ceramic oxides in YST composite anodes was evaluated on the electrochemical performance. In addition, the composite anode with low content of nickel was prepared by the impregnation method, and the performance stability was investigated in flowing hydrogen or methane fuels.

* Corresponding author. Tel.: +81 75 383 2519; fax: +81 75 383 2520.
E-mail address: eguchi@scl.kyoto-u.ac.jp (K. Eguchi).

0378-7753/$ – see front matter © 2011 Elsevier B.V. All rights reserved.
doi:10.1016/j.jpowsour.2011.12.036

2. Experimental

The composite oxide of YST with a composition of $Y_{0.08}Sr_{0.88}TiO_3$ was synthesized from the commercial reagents of $Y(CH_3COO)_3{\cdot}4H_2O$ (Wako Pure Chemical Industries), $Sr(CH_3COO)_2{\cdot}0.5H_2O$ (Wako Pure Chemical Industries), and TiO_2 (Aldrich) following the same procedure as the previous study [10]. The starting materials were mixed in distilled water and then dried. The obtained powder was calcined at 1200 °C for 5 h in air. The powders of YSZ (8 mol% Y_2O_3–ZrO_2; Tosoh Corp.) and SDC ($Ce_{0.8}Sm_{0.2}O_{1.9}$) were applied as ion-conductive oxides. The SDC powder was prepared by the ammonia co-precipitation technique starting with the solution of cerium nitrate ($Ce(NO_3)_3{\cdot}6H_2O$; Wako Pure Chemical Industries) and samarium nitrate ($Sm(NO_3)_3{\cdot}6H_2O$; Wako Pure Chemical Industries). The as-precipitated powder was subsequently calcined at 900 °C for 2 h. The composites of YST and the ion conductors were prepared to be 50 wt% of YST by ball-milling overnight before firing in air at 1400 °C for 5 h. For the addition of Ni catalyst, the composite powders were impregnated with an aqueous solution of $Ni(NO_3)_2{\cdot}6H_2O$ (Wako Pure Chemical Industries), followed by thermal decomposition at 850 °C in air to form the resultant composite with 10 wt% of NiO loading. The crystalline phase of the as-prepared powders was determined by X-ray diffraction using Cu Kα radiation (XRD, Rigaku Ultima IV).

Thermal expansion of the rectangular-shaped specimens of YST, SDC, YST–SDC, and YST–YSZ composites was measured from room temperature to 1000 °C with a heating rate of 10 °C min^{-1} in a hydrogen atmosphere, using a thermomechanical analyzer (TMA-50, Shimadzu). The samples were prepared by cold-isostatic pressing and then firing in air at 1400 °C for 5 h. The electrical conductivity of the composite was evaluated as a function of temperature using a rectangular lump with a DC four-probe method at 300–1000 °C (potentiostat/galvanostat: Solartron Analytical 1470E) in various atmospheres including oxygen, and dry and humidified (3% H_2O) hydrogen. The sample was cold-isostatically pressed at 200 MPa and then fired at 1400 °C for 5 h in air. The relative density of the samples measured by the *Archimedes method* was approximately 88%. The measurement was conducted in the heating process after holding the sample for 30 min in the respective conditions.

For the preparation of single cells, the anode composite powders (with or without NiO impregnation) were mixed with polyethyleneglycol to prepare the slurries. The slurry was screen-printed on YSZ disk (thickness: 500 μm, Tosoh) and fired at 1400 °C for 5 h in air. The perovskite type oxide of $(La_{0.8}Sr_{0.2})_{0.98}MnO_3$ (LSM) was applied as a cathode in the form of slurry on the other side of YSZ before firing at 1150 °C in air for 5 h. The effective area of both electrodes was 0.28 cm^2. Platinum wire was attached as a reference electrode to surround the side edge of YSZ disk, fixed with Pt paste, and fired at 900 °C for 2 h in air.

The electrochemical performance was evaluated with a supply of humidified hydrogen (3% H_2O) or methane (CH_4—H_2O—N_2, steam to carbon ratio ($S\,C^{-1}$) = 0.1) as a fuel. Humidified methane with a low steam to carbon ratio was supplied to accelerate the carbon deposition and to observe the tolerance. When the fuel composition is fixed, carbon formation can be thermodynamically predicted by using the C—H—O diagram; *i.e.*, the carbon deposition occurs by feeding the fuel with $S\,C^{-1} < 1.0$ at 1000 °C. The fabricated cell was attached to an alumina tube and sealed with a glass sealant. The anode was exposed to humidified hydrogen or methane–nitrogen–steam gaseous mixture in a flow rate of 100 ml min^{-1} and oxygen was fed to the cathode as an oxidant at the same flow rate. Prior to the cell testing, the anode was reduced for 30 min in a hydrogen atmosphere to reduce the composite anode. The performance stability was evaluated by discharging at a constant current density of 0.05 A cm^{-2} for 20 h. The electrochemical

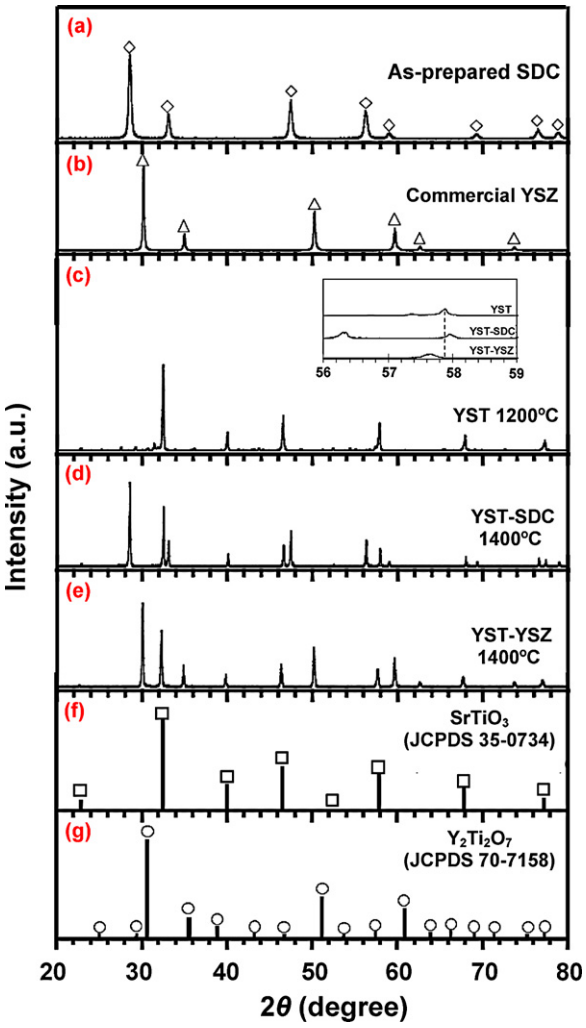

Fig. 1. XRD patterns of as-prepared SDC (a), commercial YSZ (b), YST calcined at 1200 °C (c), YST–SDC calcined at 1400 °C (d), YST–YSZ calcined at 1400 °C (e), and diffraction standards of $SrTiO_3$ and $Y_2Ti_2O_7$ (f) and (g). Inset figure shows the magnified patterns of YST, YST–YSZ and YST–SDC composites.

property was analyzed by potentiostat/galvanostat (Solartron Analytical 1470E) and frequency response analyzer (Solartron Analytical 1400). AC impedance spectra were obtained under the open-circuit condition in the frequency range of 0.1 Hz–1 MHz. The microstructures of the anode surface were observed by a scanning electron microscope (SEM, Carl Zeiss, NVision40) equipped with an energy-dispersive-X-ray spectrometer (EDX).

3. Results and discussion

3.1. Evaluation of crystal structure of the composites

Fig. 1 shows XRD patterns of the as-prepared YST powder and the composites of YST with two different ceramic oxides sintered at 1200 °C and 1400 °C in air for 5 h, respectively. Since the solubility of Y^{3+} in $SrTiO_3$ is restricted, the excess amount of Y in the system results in the formation of a trace of undesired phases of $Y_2Ti_2O_7$ and TiO_2 [17]; however, the difference in sintering atmosphere, especially oxygen partial pressure, should affect the resulting crystalline phases. In this study, the XRD pattern of YST sintered in air was closed to the desired cubic perovskite-type $SrTiO_3$ (JCPDS Card No. 35-0734) with a trace of $Y_2Ti_2O_7$ (JCPDS Card No. 70-7158). No apparent reaction products were observed in YST–SDC and YST–YSZ composite powders after sintering at 1400 °C. The

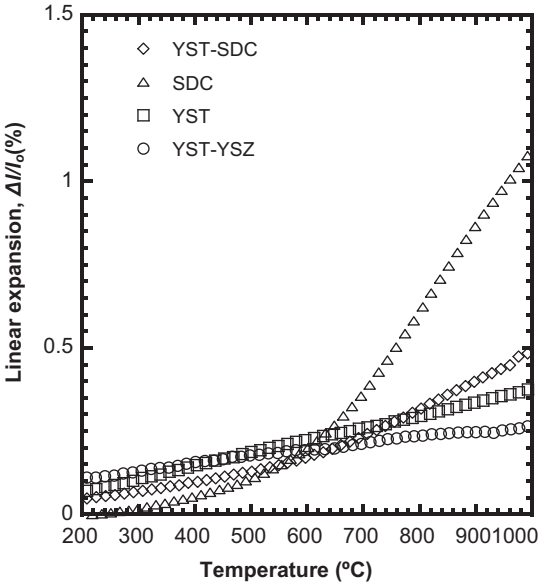

Fig. 2. Linear expansions of SDC, YST, YST–SDC, and YST–YSZ composites in a hydrogen atmosphere.

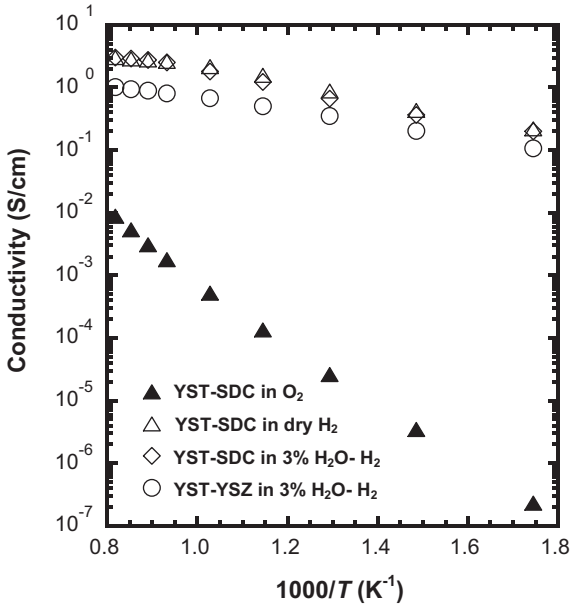

Fig. 3. Temperature dependence of electrical conductivity of YST–SDC and YST–YSZ composites measured by the DC four-probed method in oxygen, dry and humidified (3% H_2O) hydrogen.

XRD patterns were individually ascribable to those of YST and the corresponding additive oxides, and no diffraction lines of $Y_2Ti_2O_7$ phase were observed. However, a slight shifting of the diffraction peaks of YST in the composites was observed as shown in the inserted figure in Fig. 1. Comparing with YST powder, the peaks of YST appeared to displace slightly at the lower and higher diffraction angle in the composites of YST–SDC and YST–YSZ, respectively. The diffraction peaks of YSZ and SDC were also slightly shifted to the higher and lower angle in the composites of YST–SDC and YST–YSZ, respectively. In the similar system, Fu et al. reported the transition of the diffraction peaks of YST and YSZ in YST–YSZ composite after sintering at 1400 °C in Ar/H_2, which was attributed to the elemental inter-diffusion between these components [18]. Consequently, a slight change of lattice parameters of YST was confirmed from $a = 3.8992$ Å to $a = 3.9147$ Å and $a = 3.8955$ Å for the composites of YST–SDC and YST–YSZ, respectively, indicating the elemental inter-diffusion between these two components at the elevated temperature.

3.2. Mechanical and electrical characterizations

Fig. 2 shows the linear expansion of SDC, YST, YST–SDC, and YST–YSZ composites as a function of temperature in a hydrogen atmosphere. The expansion of the samples was evaluated by comparing the increment in length with the initial length (l_0) during the heating process with a ramp rate of 10 °C min^{-1}. The samples of YST and YST–YSZ expanded almost linearly in the temperature range of 100–1000 °C. The expansion of SDC was found to accelerate sharply as compared to YST and YST–SDC composite in the higher temperature region (600–1000 °C). It has been reported that the increase of slope at high temperatures indicated the formation of oxygen vacancy by the loss of lattice oxygen [19]. Interestingly, the thermal expansion of YST–SDC and YST–YSZ composites was close to that of YST. In addition, it is accepted widely that thermal expansion behavior of YST is similar to that of YSZ electrolyte [16]. Consequently, the composites of YST–SDC and YST–YSZ are compatible with YSZ electrolyte as far as thermomechanical property is concerned.

Additionally, anode materials with high electrical conductivity are preferable to the fuel cell environment. Fig. 3 shows the electrical conductivity of YST–SDC and YST–YSZ composites determined by the DC four-probe method in different atmospheres at 300–1000 °C. The electrical conductivity of the samples increased with the elevation of temperature. The composite of YST–SDC showed the higher conductivity than the composite of YST–YSZ in the reducing atmosphere. This is mainly attributable to the excellent ionic and electronic conductivity of SDC in the composite. However, in an oxygen atmosphere, the conductivity of YST–SDC composite was relatively lower than those in reducing atmospheres. Upon reduction of YST, oxygen was released from the crystal lattice leaving oxygen vacancies and electrons. As a consequence, the charge compensation led to the conversion of Ti^{4+} ions to form Ti^{3+} [6], enhancing the electronic conductivity in reducing conditions. Moreover, samaria-doped ceria shows the high electronic conductivity (>0.2 S cm^{-1} at 800 °C) due to a mixed Ce^{4+}/Ce^{3+} valence state in reducing atmospheres [20]. These excellent characteristics of SDC component would lead to the higher electrochemical performance of YST–SDC anode as compared with YST–YSZ anode. Ikebe et al. reported a continuous increase in the electrical conductivity of YST to 7.2 S cm^{-1} during reduction in a hydrogen atmosphere at 1000 °C for 100 h [10]. The YST–YSZ composite in this study exhibited a conductivity of 1.6 S cm^{-1} in dry hydrogen at 1000 °C. This lower conductivity was attributable to the shorter reduction period and the poor electrical conductivity of SDC.

3.3. Evaluation of the electrochemical performance

The composite powders were applied as anodes to evaluate the electrochemical performance of the single cells. Fig. 4 shows *I–V* and *I–P* characteristics of single cells with different anodes at 1000 °C in humidified hydrogen (3% H_2O) and oxygen as fuel and oxidant, respectively. The superior performance of *ca.* 100 mW cm^{-2} was achieved for the cell with YST–SDC anode, while the cell with YST–YSZ anode showed the power density of *ca.* 60 mW cm^{-2}. The lower performance was ascribed to the inferior catalytic activity of YST–YSZ anode. Impedance spectra of the respective anodes measured at the open-circuit condition are depicted in Fig. 5. The impedance spectrum of YST–YSZ anode was characterized by the dominant arc at the low frequency. For

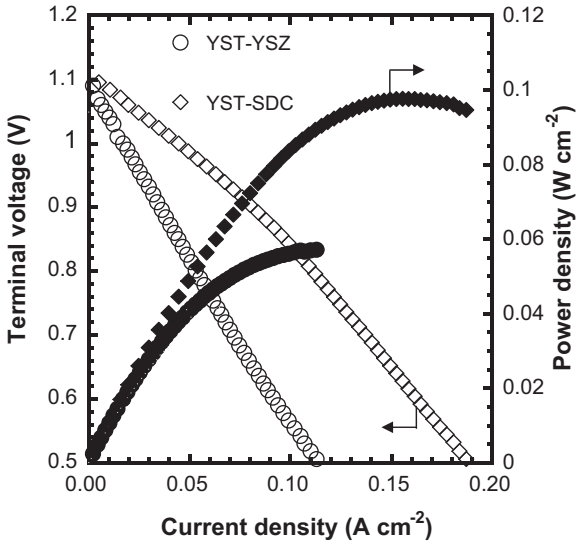

Fig. 4. *I–V* (open) and *I–P* (filled) characteristics of the single cells with YST–YSZ and YST–SDC anodes operated at 1000 °C in humidified hydrogen (3% H_2O) and oxygen (100 ml min^{-1}) as an oxidant. Cathode: LSM, electrolyte: YSZ.

LST-GDC anodes with various mixing ratios, Yoo et al. have reported that the high polarization resistance was possibly attributable to the low ionic conductivity or the poor catalytic activity [21]. In the present work, the higher ionic and electronic conductivity, and catalytic activity of SDC would promote the electrochemical hydrogen oxidation. As this consequence, the low frequency arc of YST-based composite anodes was substantially reduced in size by the use of SDC. This result is in accordance with the earlier work on LST–CeO_2 composite anodes; the low frequency arc decreased with increasing CeO_2 content up to 50 wt% [16]. Doped and undoped ceria is an active electrocatalyst for the fuel oxidation along with a unique feature of mixed ionic and electronic conduction in reducing conditions as a promising SOFC anode material [22].

3.4. Electrochemical performance of the composites incorporated with Ni catalyst

Since the electrocatalytic activity of the ceramic composites is not high as compared with the conventional Ni-based materials, the addition of catalytic material is required. Therefore, the composite powders of YST–SDC and YST–YSZ were impregnated with nickel nitrate to achieve 10 wt% of NiO in the composites. After the heat treatment at 850 °C, as-received powders were

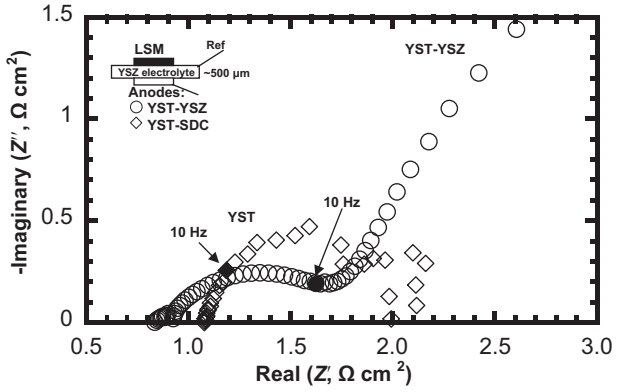

Fig. 5. Impedance spectra of YST–YSZ and YST–SDC anodes measured at 1000 °C in humidified hydrogen (3% H_2O). Cathode: LSM, electrolyte: YSZ.

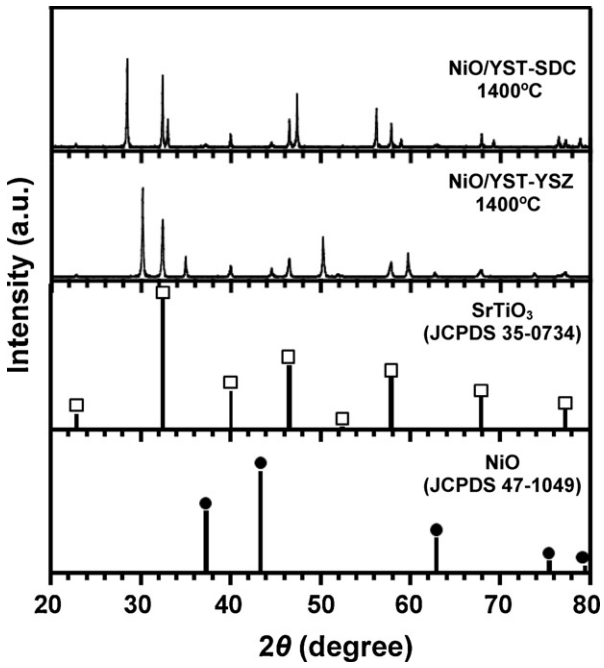

Fig. 6. XRD patterns of YST–YSZ and YST–SDC composites impregnated with 10 wt% NiO and calcined at 1400 °C in air.

subsequently applied on YSZ electrolyte and fired at 1400 °C in air for 5 h. The XRD patterns of the composite powders with NiO indicated the existence of individual phase without the chemical reaction among these components despite the calcination at 1400 °C, as shown in Fig. 6. The electrochemical performance of the cells with YST–SDC and YST–YSZ anodes impregnated with 10 wt% NiO (hereafter abbreviated as Ni/YST–YSZ and Ni/YST–SDC, respectively) was evaluated in hydrogen fuel at 1000 °C as shown in Figs. 7 and 8. The cell performance was improved significantly by the impregnated Ni catalyst in the composites. The composite anode of Ni/YST–SDC exhibited the relatively higher performance of *ca.* 140 mW cm^{-2} than Ni/YST–YSZ (*ca.* 115 mW cm^{-2}). This higher performance was ascribable to the excellence in both

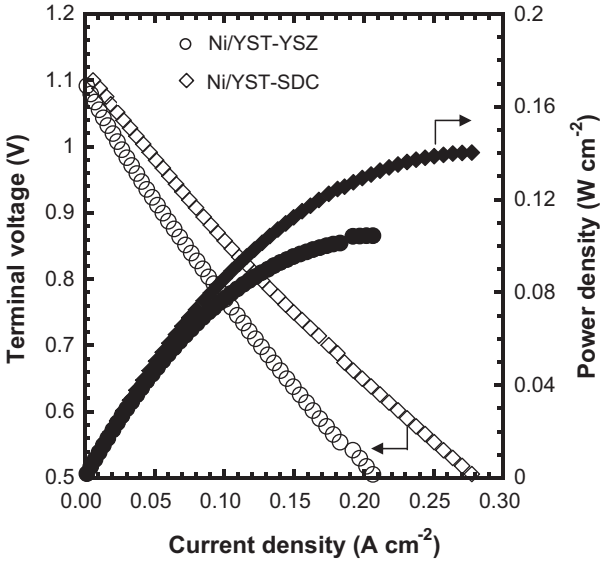

Fig. 7. *I–V* (open) and *I–P* (filled) characteristics of the single cells with Ni/YST–YSZ and Ni/YST–SDC anodes operated at 1000 °C in humidified hydrogen (3% H_2O). Cathode gas: oxygen (100 ml min^{-1}). Cathode: LSM, electrolyte: YSZ.

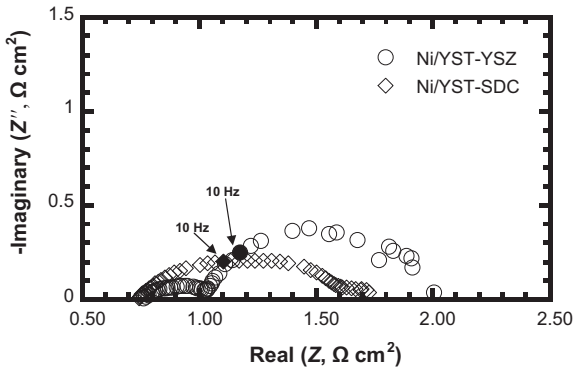

Fig. 8. Impedance spectra of Ni/YST–YSZ and Ni/YST–SDC anodes measured at 1000 °C in humidified hydrogen (3% H_2O). Cathode: LSM, electrolyte: YSZ.

electrical conductivity and electrocatalytic activity of SDC in the composite comparing with YSZ. Fig. 8 shows impedance spectra of Ni added anode materials. The significant enhancement of the electrode performance is also confirmed by the decrease in polarization resistance for the impregnated Ni anodes compared with that of without Ni anodes. This indicates that the impregnated Ni catalyst can enhance the electrocatalytic activity for the hydrogen oxidation. Since YST–SDC composite showed the higher performance than YST–YSZ composite, hereafter, the cell with YST–SDC anode was used for the further investigation.

Microstructures of Ni/YST–SDC after reduction at 1000 °C for 30 min were observed by chamber and in-lens detectors installed in the SEM column, as shown in Fig. 9(a) and (b), respectively. By EDX analysis, the bright particles with the terraced and smooth surfaces were confirmed to be mainly YST and Ni, respectively, and the dark ones were attributable to SDC in Fig. 9(b). The elemental analysis showed that the impregnated nickel particles were dispersed intensively into YST–SDC composite as shown in Fig. 9(d). Additionally, the microstructure of Ni/YST–SDC composite exhibited the good connectivity of the ionic and electronic conducting phases, leading to the high performance.

3.5. Stability in electrochemical performance

To evaluate the stability in electrochemical performance of the composite anodes, the cells were discharged at a constant current of 0.05 A cm^{-2} for 20 h in hydrogen and methane fuels as shown in Figs. 10 and 11, respectively. The results show the time courses of terminal voltage and anodic overpotential for the cells using YST–SDC and Ni/YST–SDC anodes. Without Ni addition, the higher performance was achieved in hydrogen fuel comparing with in methane at 1000 °C. The performance of the cell with YST–SDC anode was gradually degraded at 900 °C operated in hydrogen fuel, while the performance was clearly improved by an increase of temperature to 1000 °C or the addition of Ni catalyst into the composite anode. The reason for the performance deterioration is still unclear at this moment. However, the slow change of the ordering of oxygen vacancies in the donor-doped titanates was suggested as a possible reason [21]. Although the vacancy ordering in the donor-doped $SrTiO_3$ has not been elucidated thoroughly, the decline in the oxygen chemical diffusivity and the surface-exchange kinetics may be expected. In addition, the slight oxidation of the composite by the supplied water during discharge process could be suggested

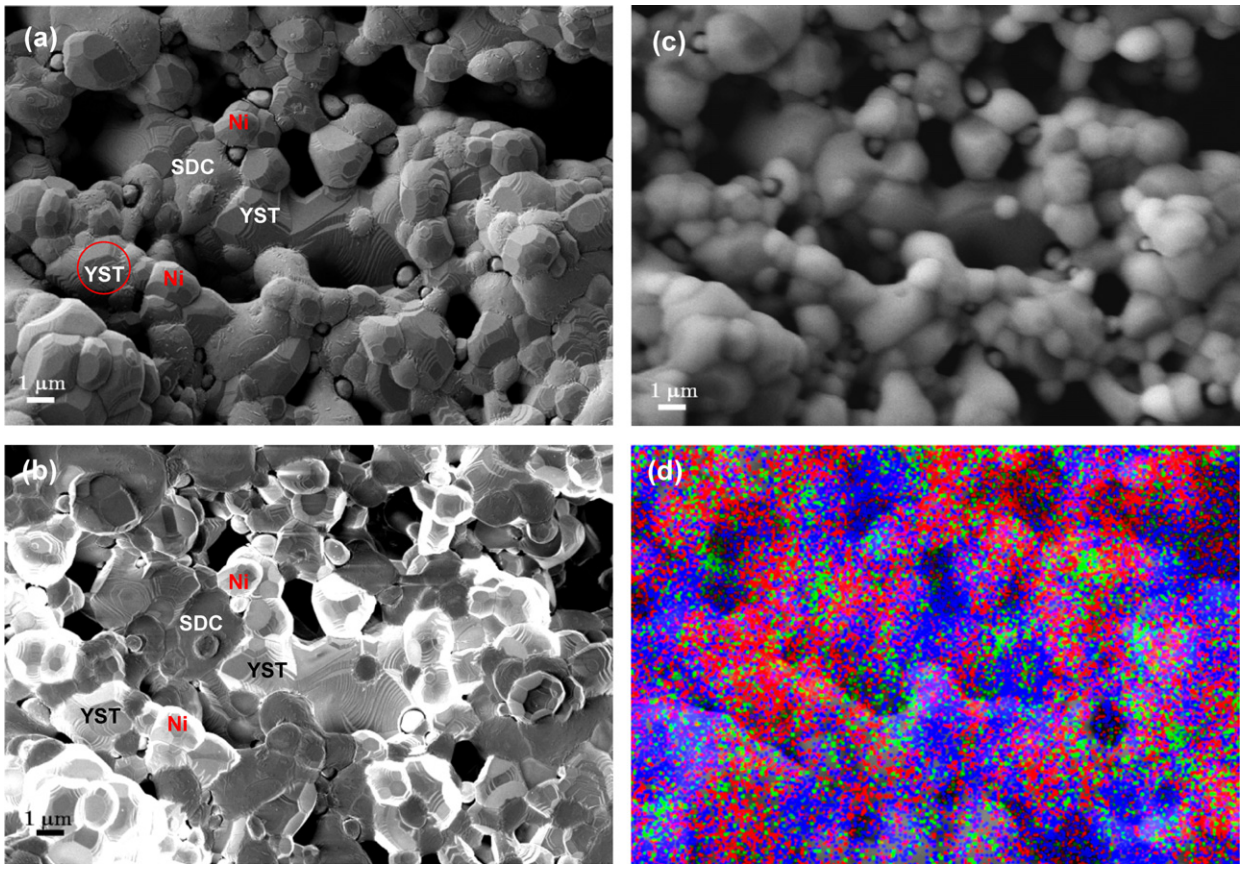

Fig. 9. SEM images of Ni/YST–SDC composites after reduction in humidified hydrogen (3% H_2O) at 1000 °C for 30 min (a)–(c) with elemental analysis (d). The secondary electron images of (a) and (b) were obtained by chamber and in-lens detectors installed in SEM column, respectively. The green, red and blue parts correspond to Ni, Ti, and Ce, respectively. (For interpretation of the references to color in this figure legend, the reader is referred to the web version of the article.)

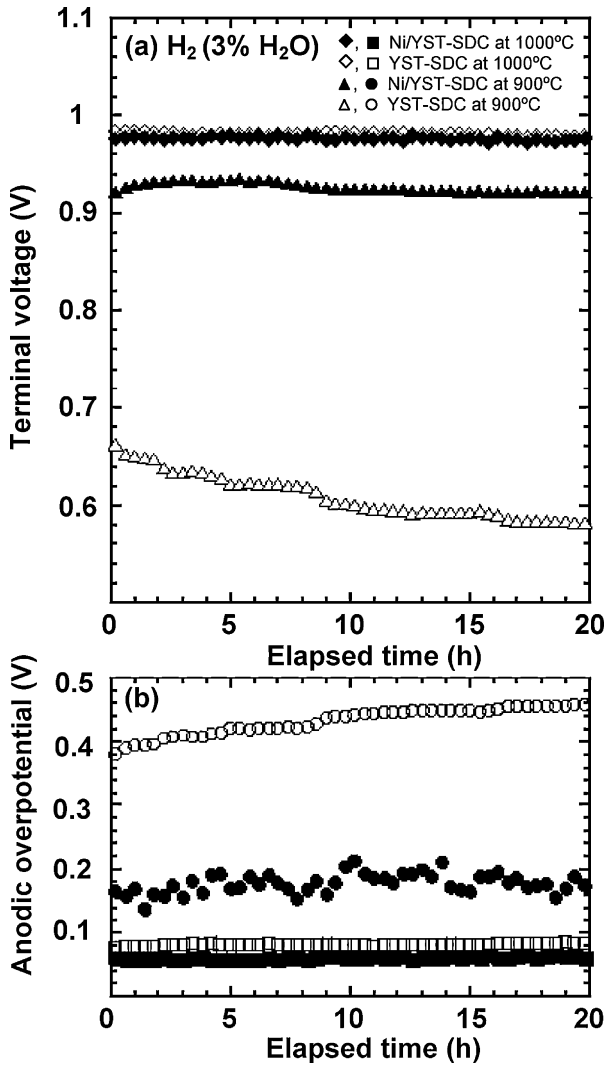

Fig. 10. Time courses of terminal voltage (a) and anodic overpotential (b) of the single cells with Ni/YST–SDC and YST–SDC operated at 900 °C and 1000 °C during a discharge at a constant current of 0.05 A cm^{-2} in humidified hydrogen (3% H_2O—H_2). Cathode gas: oxygen (100 ml min^{-1}). Cathode: LSM, electrolyte: YSZ.

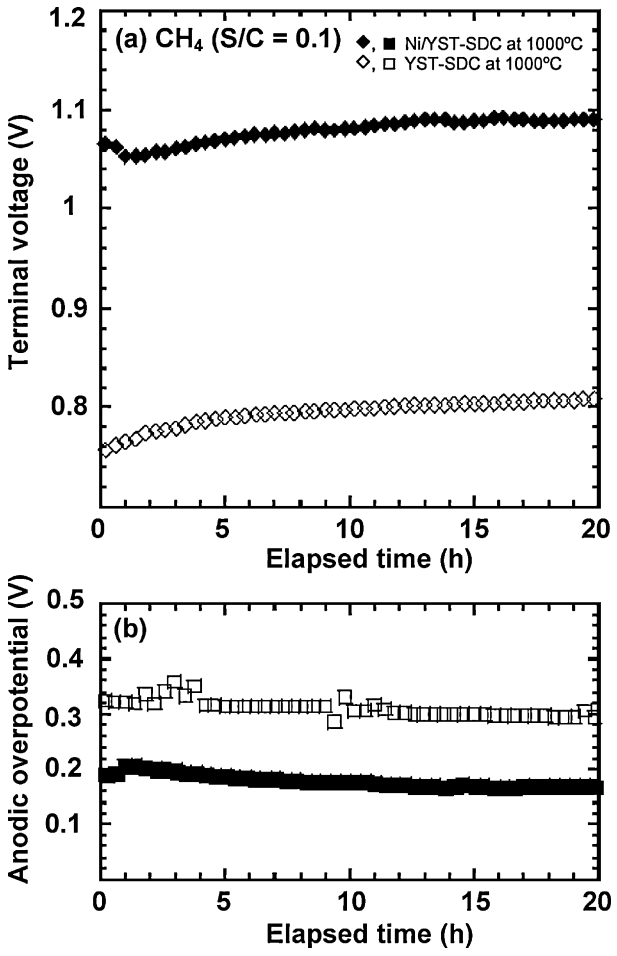

Fig. 11. Time courses of terminal voltage (a) and anodic overpotential (b) of the single cells with Ni/YST–SDC and YST–SDC operated at 1000 °C during a discharge at a constant current of 0.05 A cm^{-2} in humidified methane fuels (N_2—H_2O—CH_4, S/C = 0.1). Cathode gas: oxygen (100 ml min^{-1}). Cathode: LSM, electrolyte: YSZ.

as a reason for the performance degradation. The anodic overpotential was reduced by the addition of Ni catalyst, indicating the enhancement of the electrocatalytic activity and the increment in reaction sites of anodes. Yoo et al. [21] also reported the decrease in polarization resistance of LST-GDC anode by impregnation of Ni into the composite. Moreover, nickel is a well-known catalyst for the reforming of methane. Therefore, the improved performance under the operation with methane fuel was attributed to the increase in catalytic activity for the reforming reaction by the impregnated Ni catalyst. The OCV (data not shown) for the cell with Ni/YST–SDC anode in methane fuel was higher than that in hydrogen fuel since the coke formation can be simultaneously promoted by nickel. Considering the almost stable performance even in low-humidified methane fuel, the coke formation over Ni catalyst insignificantly had a worse impact on the cell performance. In general, the electrocatalytic activity of SDC for the methane oxidation is relatively lower than the Ni-containing anode. Accordingly, it was suggested that the addition of small amount of nickel into the composite anode could effectively enhance the electrocatalytic activity of the cell without the deterioration caused by carbon deposition even in the severe condition. From the experimental points of view, however, further development is still required to obtain excellent anode performance with stability during long-term operation.

4. Conclusions

The composite anodes based on Y-doped $SrTiO_3$ (YST) with different ceramic oxides of SDC and YSZ were prepared to evaluate the electrocatalytic performance in hydrogen and methane fuels. The composite of YST–SDC attained the excellent performance comparing with YST–YSZ composite, which was ascribable to the excellence in both electrical conductivity and electrocatalytic activity towards the oxidation of fuels for SDC. The introduction of Ni into the composite anode provided the superior electrochemical performance for the oxidation of both hydrogen and methane. Moreover, the electrocatalytic activity could be effectively enhanced by the impregnated Ni without the performance deterioration induced by carbon deposition. Although the addition of nickel showed the improvement mainly in the catalytic activity and the electrical conductivity of YST–SDC composite, it would affect the stability of YST–SDC composite due to unavoidable carbon deposition during the prolonged operation with hydrocarbon fuels. Accordingly, it is essential to limit the amount of nickel in YST–SDC composite to minimize the degradation by coke formation.

References

[1] H. Kim, S. Park, J.M. Vohs, R.J. Gorte, J. Electrochem. Soc. 148 (2001) A693.
[2] H. Kishimoto, Y.P. Xiong, K. Yamaji, T. Horita, N. Sakai, M.E. Brito, H. Yokokawa, J. Chem. Eng. Jpn. 40 (2007) 1178.
[3] N.F.P. Ribeiro, M.M.V.M. Souza, O.R.M. Neto, S.M.R. Vasconcelos, M. Schmal, Appl. Catal. A: Gen. 353 (2009) 305.
[4] J.T. Vaughey, J.R. Mawdsley, T.R. Krause, Mater. Res. Bull. 42 (2007) 1963.
[5] J.C. Ruiz-Morales, J. Canales-Vazquez, D. Marrero-lopeZ, J.T.S. Irvine, P. Nunez, Electrochim. Acta 52 (2007) 7217.
[6] O.A. Marina, N.L. Canfield, J.W. Stevenson, Solid State Ionics 149 (2002) 21–28.
[7] S. An, C. Lu, W.L. Worrell, R.J. Gorte, J.M. Vohs, Solid State Ionics 175 (2004) 135.
[8] Z.L. Zhan, S.A. Barnett, Science 308 (2005) 844.
[9] X.F. Ye, B. Huang, S.R. Wang, Z.R. Wang, L. Xiong, T.L. Wen, J. Power Sources 164 (2007) 203.
[10] T. Ikebe, H. Muroyama, T. Matsui, K. Eguchi, J. Electrochem. Soc. 157 (2010) 970.
[11] S. Hui, A. Petric, Mater. Res. Bull. 37 (2002) 1215.
[12] X. Huang, H. Zhao, W. Shen, W. Qin, W. Wu, J. Phys. Chem. Solids 67 (2006) 2609.
[13] X. Li, H. Zhao, F. Gao, Z. Zhu, N. Chen, W. Shen, Solid State Ionics 179 (2008) 1588.
[14] X.F. Sun, R.S. Guo, J. Li, Ceram. Int. 34 (2008) 219.
[15] S. Koutcheiko, Y. Yoo, A. Petric, I. Davidson, Ceram. Int. 32 (2006) 67.
[16] X. Sun, S. Wang, Z. Wang, J. Qian, T. Wen, F.Q. Huang, J. Power Sources 187 (2009) 85.
[17] S. Hui, A. Petric, J. Electrochem. Soc. 149 (2002) J1.
[18] Q.X. Fu, F. Tietz, Fuel Cells 2008 05 (2008) 283.
[19] W.X. Chen, T.L. Wen, H.W. Nie, R. Zheng, Mater. Res. Bull. 38 (2003) 1319.
[20] X. Zhang, S. Ohara, R. Maric, K. Mukai, T. Fukui, H. Yoshida, M. Nishimura, T. Inagaki, K. Miura, J. Power Sources 83 (1999) 170.
[21] K.B. Yoo, G.M. Choi, Solid State Ionics 180 (2009) 867.
[22] M. Mogensen, T. Lindegaard, U.R. Hansen, G. Mogensen, J. Electrochem. Soc. 141 (1994) 2122.